Eur. Phys. J. D **28**, 381–392 (2004)
DOI: 10.1140/epjd/e2003-00322-3

THE EUROPEAN PHYSICAL JOURNAL D

Jump conditions in hypersonic shocks

Quantitative effects of ionic excitation and radiation

C. Michaut[1,a], C. Stehlé[1], S. Leygnac[1], T. Lanz[1,2,3], and L. Boireau[1]

[1] LUTH, UMR 8102 du CNRS, Observatoire de Paris, 5 place J. Janssen , 92195 Meudon, France
[2] Department of Astronomy, University of Maryland, College Park, MD 20742, USA
[3] NASA Goddard Space Flight Center, Code 681, Greenbelt, MD 20771, USA

Received 7 April 2003 / Received in final form 3 October 2003
Published online 6 January 2004 –

Abstract. We study the quantitative effects of excitation, ionization, radiation energy and pressure, on the jump conditions in hypersonic shocks in a real gas. The ionization structure and excitation energies are calculated from the local temperature and density, using the Screened Hydrogenic Model. We assume an optically thick medium and no radiation flux through the shock front. We investigate the jump conditions in different gases and propose a phenomenological description of compression for different shock velocities. We find that the excitation energy term is the dominant term in ionized gases at low velocities. Consequently, higher shock velocities than the values predicted by standard calculations in a perfect gas must be reached in order to observe the effects of radiation in the compression ratio. Our results provide constraints for the design of future radiative shock experiments on the next generation of powerful nanosecond lasers or on Z-pinches.

PACS. 52.35.Tc Shock waves and discontinuities – 95.30.Dr Atomic processes and interactions – 95.30.Lz Hydrodynamics

1 Introduction

Radiative shocks are strong hypersonic shocks. Due to gas heating in the shock, atoms and molecules are excited, dissociated, ionized and, as a result, they radiate away some of the absorbed energy. The radiation travels faster, ahead through the shock front, and heats the unshocked media creating a radiative precursor. The presence of a radiative precursor often is the criterion which refers the shock as radiative. The total optical depth of the medium in which radiative shocks occur determines the detailed structure of the shock (see, e.g. [1]). Several characteristic regions could be distinguished in a radiative shock occurring in an optically-thin, or moderately optically-thick plasma. As mentioned above, the main characteristic zone is the radiative precursor. Just after the precursor, we find several zones where different equilibria are achieved: (1) the kinetic equilibrium for each species of particles, (2) a zone where the electronic temperature comes to equilibrium with the ionic temperature, and possibly (3) a zone where radiative equilibrium is achieved. Large departures from the Local Thermodynamic Equilibrium (LTE) are thus a typical feature of the shock region in optically thin plasmas. Conversely, the situation of optically-thick media is much simpler: the temperature remains roughly constant in the shock region, and tends to decrease slightly in the radiative precursor. In astrophysical conditions, radiative shocks occur in a wide variety of objects, at very different densities, hence in media with very different total optical depths. Examples include shocks in supernova remnants, in atmospheres and envelopes of pulsating stars [2–4], in accretion processes during star formation [5], and in exploding supernovae [6], ranging from (very) small to (very) large total optical depths. With the exception of the latter case, departures from LTE and radiative cooling are major drivers of the shock structure, in particular of the compression ratio.

Shocks and related discontinuities are a difficult numerical problem to solve in radiation hydrodynamics. It is therefore crucial to validate the computer codes which are applied to model astrophysical objects or laboratory plasmas. A major goal of recent experimental work is thus to provide benchmarks for radiation hydrodynamics codes [7]. Particular attention has been recently devoted to the experimental study of 2-D and 3-D expanding blast waves [8–10] and 1-D radiative shocks [11–13]. They show strong hydrodynamical discontinuities and radiative precursors. These experiments require high-power energy installations like high-power lasers or Z-pinches. The hydrodynamics and geometry of these shocks are quite different: the blast waves follow a point-like explosion induced

[a] e-mail: Claire.Michaut@obspm.fr

by intense ultra-short lasers. The front shock decelerates with time and can never be stationary. On the other hand, 1-D radiative shock experiments are conducted with high-energy lasers with longer duration pulses. The front shock velocity remains nearly constant. A radiative precursor develops ahead of the shock front, at higher velocities. The duration of the laser pulses generally remains too short to reach the stationary limit in the whole shock structure.

The eventual goal is to reach a regime where the whole shock structure is dominated by radiation. This objective requires to drive a shock at higher velocities than values reached in present experiments, as well as to reach the optically-thick limit. These conditions are hard to fulfill experimentally nowadays. The limited total optical depths in current experimental settings imply that radiative shock structures in the laboratory are more or less dominated by radiative losses.

In order to design such fully radiative 1-D shock experiments, Bouquet et al. [14] developed an analytical model of stationary radiative shocks, assuming a perfect gas, one-dimensional geometry, large total optical depth, LTE and the diffusion approximation to describe the radiation transport. Relevant to the experimental set-up, Bouquet et al. showed that shocks are more radiative when the ambient medium is at low pressure and is constituted of heavy gas, for example xenon. Following the usual approach in radiation hydrodynamics, Bouquet et al. assumed a perfect gas, neglecting thus the excitation and ionization of the gas. In an experimental set-up to produce radiative shocks, xenon will be ionized several times and a significant fraction of the mechanical energy may therefore be used to excite and ionize the gas. This effect may actually dominate the radiation effect.

In this paper, we revisit the assumption of the perfect gas, quantitatively estimating the effect of excitation and ionization, and of radiative energy and pressure, on the post-shock conditions. We model radiative shocks for different initial conditions. We solve the Generalized Rankine-Hugoniot (GRH) relations for ionized gases, accounting for radiative energy and radiation pressure assuming LTE. Whereas the basic equations were already written down by Zel'dovich and Raiser [15], only limited computations for special cases were previously reported. For example, the effect of radiative energy and pressure was studied for perfect gases by [16] and later by [14]; the effect of excitation and ionization was reported on for specific gases, like nitrogen and oxygen gases [17] but without radiation effects, or for hydrogen at high shock velocities, including radiative effects [18]. However, no extensive and quantitative calculations were performed to explore the role of radiation in real gases in different conditions. Our study complements the work of Nieuwenhuijzen et al. [19], who proposed a way to resolve the GRH relations using a tabulated Equation of State (EOS). Our approach differs in that we calculate relevant atomic quantities on-the-fly, and focus primarily on deriving the conditions for different gases where radiation plays a role through the shock front. We adopt a relatively simple atomic description, the Screened Hydrogenic Model [20,21], which is a reasonable description for multiple-charged rare gases. We choose to focus our study on rare gases because they can be easily handled in experimental conditions. In astrophysical settings, hydrogen is the most important case. We will consider a detailed atomic and molecular description of hydrogen in a subsequent paper.

Our assumptions are as follows: large total optical depth, with very small photon mean path and thus negligible radiative flux; LTE; stationarity; one-dimension geometry; pure gases; and no magnetic fields. Our model therefore provides the conditions in the post-shock region relative to the initial conditions in the pre-shock region, that is essentially the compression ratio. We aim at assessing the effect of excitation, ionization, and radiation, on this compression ratio, but not at describing the detailed structure of the shock. This model should not be applied blindly to astrophysical or experimental settings where the total optical depth is generally not as large as assumed here, where the radiative flux might be important, and LTE breaks down in the shock region. Our intention is to keep the model simple as to assess the assumption of perfect gas made in most radiation hydrodynamics calculations. For real gases, we will indeed show that the compression ratio is significantly modified and that the radiative effects in the compressed gas arise at higher shock velocities. In the next stage, we will use this model as the starting solution of a more realistic model of radiative shocks that include a detailed treatment of radiation transport and departures from LTE.

This paper is organized as follows. In Section 2, we present the Generalized Rankine-Hugoniot relations which include the radiation energy and pressure terms. The atomic model adopted for calculating the relevant microscopic quantities is described in Section 3. The characteristics of shocks in various gases is presented in Section 4, and the radiative effects are further discussed in Section 4.3.

2 Jump relations

In this section, we introduce the Generalized Rankine-Hugoniot equations which include the contributions of radiation energy, E_{rad}, and pressure, P_{rad}. These equations, derived for a stationary 1D shock, give the hydrodynamical quantities ahead and behind the shock discontinuity [15]. We first apply these equations to the case of a perfect gas with polytropic index γ.

Hereafter, ρ is the volumic mass density, P_{th} the thermal pressure, T the temperature, and h the massic enthalpy. We write the three usual continuity equations (mass, momentum and energy) in a coordinate system that moves with the shock front, at the velocity $-u_1$

$$\rho_2 u_2 = \rho_1 u_1 \tag{1}$$

$$\rho_2 u_2^2 + P_{th_2} + P_{rad_2} = \rho_1 u_1^2 + P_{th_1} + P_{rad_1} \tag{2}$$

$$\rho_2 u_2 \left[h_2 + \frac{1}{2}u_2^2\right] + u_2 \left[P_{rad_2} + E_{rad_2}\right] = \rho_1 u_1 \left[h_1 + \frac{1}{2}u_1^2\right] + u_1 \left[P_{rad_1} + E_{rad_1}\right] \tag{3}$$

where the indices 1 and 2 stand for the unshocked and shocked parts of the gas, respectively. Therefore, u_1 is the velocity of the unshocked matter relative to the shock front. The contribution of the radiative fluxes are neglected, because we solve for quantities far from the shock front in an optically-thick medium. The radiation energy and pressure are taken at radiative equilibrium. This approximation is only correct at high densities when the opacity is large and the diffusion approximation is valid for the radiative flux [1]. We assume this approximation as an initial description for this paper, deferring an improved treatment of the radiative transfer from the shock to the precursor to a future paper. In our description, we have

$$P_{rad} = \frac{1}{3}E_{rad} = \frac{1}{3}a_r T^4. \quad (4)$$

2.1 Perfect gas case

In the case of a polytropic perfect gas, the thermal pressure and the enthalpy are respectively given by

$$P_{th} = \rho\frac{RT}{A} \quad \text{and} \quad h = \frac{\gamma}{\gamma-1}\rho\frac{RT}{A} \quad (5)$$

where A is the atomic mass of the gas, and the molar gas constant R is related to the Boltzmann constant k, and to the number n of particles per unit of volume by $R = nkA/\rho$. The preceding equations then become

$$\rho_2 u_2 = \rho_1 u_1 \quad (6)$$

$$\rho_2 u_2^2 + \rho_2\frac{RT_2}{A} + \frac{1}{3}a_r T_2^4 = \rho_1 u_1^2 + \rho_1\frac{RT_1}{A} + \frac{1}{3}a_r T_1^4 \quad (7)$$

$$\rho_2 u_2\left[\frac{\gamma}{\gamma-1}\rho_2\frac{RT_2}{A} + \frac{1}{2}u_2^2\right] + u_2\frac{4}{3}a_r T_2^4 = \rho_1 u_1\left[\frac{\gamma}{\gamma-1}\rho_1\frac{RT_1}{A} + \frac{1}{2}u_1^2\right] + u_1\frac{4}{3}a_r T_1^4. \quad (8)$$

The Mach number M is the ratio of the shock speed u_1 to the sound velocity in the unshocked material, which is given for a perfect gas by

$$v_{s,perf} = \sqrt{\frac{\gamma RT}{A}}, \quad (9)$$

that is $v_{s,perf} = 13$ km s^{-1} for $kT = 1$ eV, $\gamma = 5/3$, and $A = 1$ g/mol (atomic hydrogen gas).

As described by Bouquet et al. [14], the variations of the compression ratio with the shock velocity u_1 show a plateau close to the asymptotic compression ratio without radiation, $\rho_2/\rho_1 = (\gamma+1)/(\gamma-1)$ (i.e., $\rho_2/\rho_1 = 4$ for $\gamma = 5/3$). At higher shock velocities, radiative effects appear and the compression ratio increases towards the theoretical asymptotical limit of 7. This is illustrated in Figure 1 for hydrogen, assuming an initial density $\rho_1 = 5\times10^{-4}$ g cm^{-3} and different initial temperatures T_1.

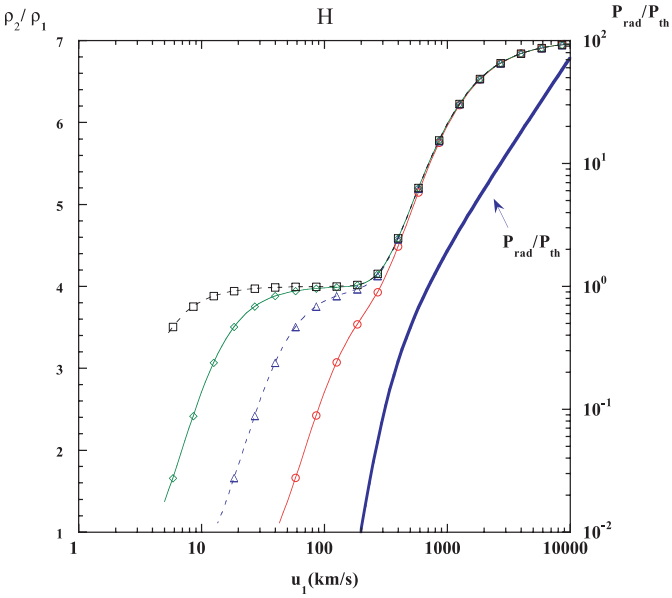

Fig. 1. Compression ratio, ρ_2/ρ_1, and P_{rad}/P_{th} for hydrogen, considered as a perfect gas with $\gamma = 5/3$, for different initial temperatures T_1 ($kT_1 = 0.01$ eV (dashed lines, squares), 0.1 eV (diamond), 1 eV (dashed lines, triangles) and 10 eV (circles), versus the shock velocity u_1 in km s^{-1}. The initial density ρ_1 is equal to 5×10^{-4} g cm^{-3}. The curves P_{rad}/P_{th} for the different initial temperatures in bold are indistinguishable on the graphic scale.

This figure shows together the compression ratio ρ_2/ρ_1 and the ratio of radiative to thermal pressure.

The shock velocity, $u_1 = u_{rad}$, for which the radiative and thermal pressures are equal is independent of γ and is given by [14]:

$$u_{rad} = 7^{7/6}\left(\frac{R}{A}\right)^{2/3}\left(\frac{\rho_1}{a_r}\right)^{1/6}. \quad (10)$$

This relation is valid at high Mach number (thus for a compression ratio close to 7). For hydrogen and an initial density of $\rho_1 = 5\times10^{-4}$ g cm^{-3}, we note indeed that u_{rad} is usually independent of the initial temperature T_1. We choose initial conditions ρ_1 and T_1 that correspond to the experimental conditions in xenon [11]. The variations of u_{rad} with the initial temperature will be discussed in Section 4.3.

In Figure 2, we report the variations of the temperature T_2 in the shocked gas versus the shock velocity. This temperature varies, as indicated in [14], as u_1^2 at low velocities and as $u_1^{1/2}$ at high velocities, whereas it would also vary as u_1^2 at high velocities if the radiative terms were neglected. Radiative effects reduce the heating of the gas at high shock velocities. In Figure 3, we show the variation of the compression ratio and the ratio of radiative to thermal pressures for hydrogen and xenon versus the shock velocity for the same initial density (5×10^{-4} g cm^{-3}) and $kT_1 = 10$ eV. At each velocity u_1, we verify that the radiative effects are larger in xenon than in hydrogen: P_{rad}/P_{th} is larger in xenon by about two orders of

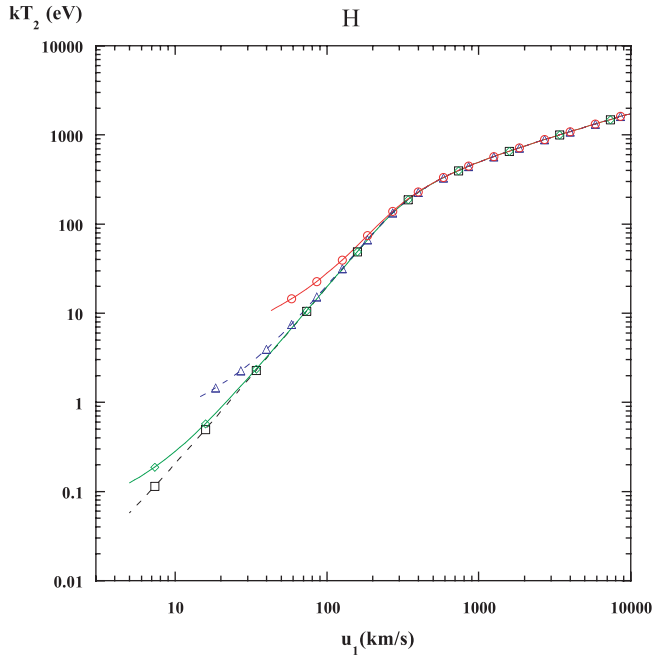

Fig. 2. Same as Figure 1 for the temperature T_2 (in eV) of the compressed gas.

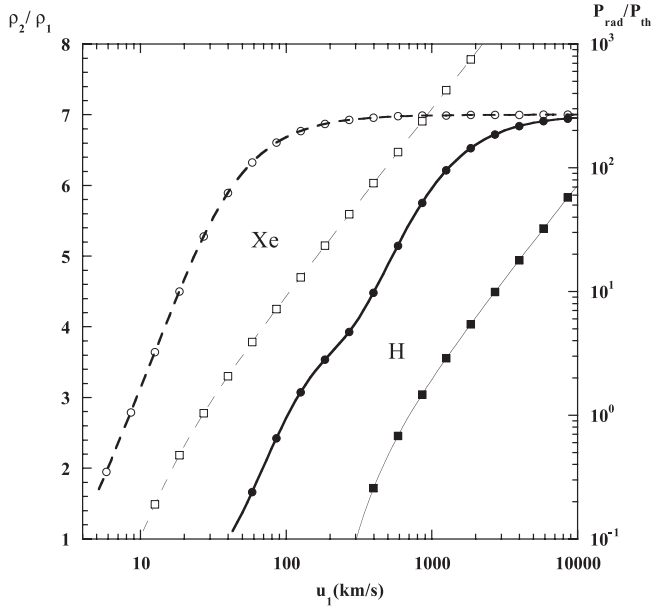

Fig. 3. ρ_2/ρ_1 (circles) and P_{rad}/P_{th} (squares) versus the shock velocity u_1 ($\mathrm{km\,s^{-1}}$) for hydrogen (full line, full markers) and xenon (dashed line, empty markers), both considered as perfect gases with $\gamma = 5/3$, for an initial temperatures $kT_1 = 10$ eV and density $\rho_1 = 5 \times 10^{-4}$ $\mathrm{g\,cm^{-3}}$. The two compression ratio curves converge towards 7 at high shock velocities.

magnitude, which follows from the higher atomic mass of xenon ($A = 131$). The kinetic energy is larger at a given velocity for the heavier element, resulting in more warming and in larger radiative effects.

From this simple description of a radiative shock in a perfect gas, we conclude that the radiative effects modify the shock structure at high shock velocities, enhancing the compression ratio on one hand, and changing the dependency of the shocked gas temperature with the shock velocity (in $u_1^{1/2}$ instead of in u_1^2 without radiative effects) on the other hand. In this approach, the radiative effects (quantified by the ratio P_{rad}/P_{th}) are predicted to be larger for heavier gases (at constant initial volumic mass density).

This description assumes that the mechanical energy taken from the piston is used to compress and heat the gas. It neglects the competitive effect of excitation and ionization processes which may also take a large fraction of the mechanical energy, resulting in a lesser increase of temperature and smaller radiative effects (which vary as T^4).

2.2 Generalized Rankine-Hugoniot for ionized gas

We now consider the case of an atomic gas (atomic number $\mathcal{Z}$) which can be partially ionized. We denote by $\langle Z \rangle$ the mean ionization stage which is also the ratio of the number of electrons to the number of ions. The excitation energy per atom is denoted by ϵ_{exc}. We adopt hereafter the energy of the fully ionized isolated element as the reference "zero" energy. Let α and i denote the ionization stages (0 for neutral, $\mathcal{Z}$ for the fully ionized atom) and atomic levels, respectively. Finally, let $\mathcal{P}_{\alpha,i}$ be the fraction of species in ionization stage α and atomic state i having also energy $E_{\alpha,i}$. One has

$$\langle Z \rangle = \sum_{\alpha=0,\mathcal{Z}} \alpha \mathcal{P}_{\alpha,i} \tag{11}$$

$$\epsilon_{exc} = \sum_{\alpha,i} \mathcal{P}_{\alpha,i} E_{\alpha,i}. \tag{12}$$

The level populations $\mathcal{P}_{\alpha,i}$ are derived from Boltzmann statistics assuming LTE.

The thermal pressure can be decomposed into ionic and electronic contributions. The ratio between these two contributions is equal to $\langle Z \rangle$. The enthalpy now includes the contribution due to the excitation energy, ϵ_{exc}. One has

$$P_{th} = \rho \frac{RT}{A}(1 + \langle Z \rangle) \tag{13}$$

$$h = \frac{5}{2}\rho \frac{RT}{A}(1 + \langle Z \rangle) + \epsilon_{exc}. \tag{14}$$

The three-equation system therefore becomes

$$\rho_2 u_2 = \rho_1 u_1 \tag{15}$$

$$\rho_2 u_2^2 + \rho_2 \frac{RT_2}{A}(1 + \langle Z \rangle_2) + \frac{1}{3} a_r T_2^4 = \rho_1 u_1^2 + \rho_1 \frac{RT_1}{A}(1 + \langle Z \rangle_1) + \frac{1}{3} a_r T_1^4 \tag{16}$$

$$\rho_2 u_2 \left[\frac{5}{2}\rho_2 \frac{RT_2}{A}(1 + \langle Z \rangle_2) + \epsilon_{exc,\,2} + \frac{1}{2}u_2^2\right] + u_2 \frac{4}{3} a_r T_2^4 = \rho_1 u_1 \left[\frac{5}{2}\rho_1 \frac{RT_1}{A}(1 + \langle Z \rangle_1) + \epsilon_{exc,\,1} + \frac{1}{2}u_1^2\right] + u_1 \frac{4}{3} a_r T_1^4. \tag{17}$$

We recall that $\langle Z \rangle$ and ϵ_{exc} both depend on ρ and T, and are calculated for each necessary couple (ρ, T) used during the solution process. Consequently, the equations are strongly nonlinear, and one needs to build an iterative algorithm that uses convergence criteria which automatically adapt to the stiffness of the system.

The differences between the cases of perfect and ionized gas come from the ionization degree and excitation processes that appear in the $\langle Z \rangle$ and ϵ_{exc} terms. We shall illustrate the role played by these two contributions. Our aim is to derive the general trends due to both the radiation and the ionization effects in the generalized Rankine-Hugoniot equations. In an initial stage, we use simple efficient procedures to compute the excitation energy and the equation of state. In particular, the equation of state is given by the perfect gas law. This approximation is valid for a large range of density and temperature conditions, but fails at high densities. This issue may concern the conditions in the shocked gas at very high shock velocities and/or at high initial densities. However, at high shock velocities, the radiation effects tend to dominate the thermal pressure, and the details of the equation of state are therefore not important. The resulting effects of departure from the perfect gas equation of state will be discussed in a future paper. The goal of this work is to highlight the radiative effects and the importance of microscopic parameters on the shock structure, resulting in large differences in the compression ratios between a perfect gas and a more realistic gas where ionization is taken into account.

3 Atomic physics

This study concerns pure atomic gases like hydrogen, helium, neon, argon, krypton and xenon, which are good candidates for laboratory experiments. Among these gases, hydrogen is very interesting for two reasons. First, many radiative shocks occur in astrophysics, and hydrogen is the dominant cosmic species. As radiation is treated in the blackbody approximation, contributions from heavier, less abundant species to the radiative flux, energy and pressure are not relevant. Moreover, the equation of state of such mixtures is close to the case of pure hydrogen. Second, the simple atomic structure of hydrogen allows to better understand the relevant physics before addressing more complicated gases.

Throughout this paper, we adopt an ion-sphere model: the Screened Hydrogenic Model (SHM) which allows us to compute very quickly all necessary atomic quantities for gases having a very large number of electrons. A more detailed description provided by standard atomic packages requires impracticable computer time and memory in our context. In the Screened Hydrogenic Model [20,21], the bound electrons of the ion with nuclear charge Z are distributed in shells characterized by the principal quantum number n. The effects of the angular orbital momentum l are not included. The effects of exchange and interactions between the electrons are included through screening constants [22]. On average, the action on one electron by the other electrons consists in a screening of the nuclear charge. Each bound state is characterized by an integer population of electrons in this state and by an effective charge. Density effects are qualitatively incorporated by a simple model of lowering the ionization energy. This model stipulates that the lowering of the ionization energy is proportional to the number of ions in the considered ionic stage. For ionization stage α (0 for the neutral), the ionization lowering energy is related to the volumic ρ and atomic (A) masses as described in [23]:

$$\Delta E_\alpha \,[\mathrm{eV}] \simeq 35\,[\mathrm{eV\,cm}]\;\alpha\;\left(\rho\;\left[\mathrm{g\,cm^{-3}}\right]/A\,[\mathrm{g}]\right)^{1/3}. \quad (18)$$

Initially, we have adopted the SHM due to its very advantageous coupling to hydrodynamics calculations. However, the predictions of spectroscopic quantities is then only qualitative, and this model is not suitable to predict or interpret spectra, which is not our purpose here. In future stages of our study, we plan to use an improved atomic description for light elements and molecules that are most important in astrophysical phenomena. At this initial stage, however, detailed physical atomic models are too unwieldy for our approach that aims at comparing various gases and the effects of the atomic mass.

To illustrate the SHM, the ionization energies of various ionization stages are reported in Figure 4 for different rare gases. The Saha-Boltzmann equations allow us to compute the ionization stage of the plasma. We have tested the accuracy of this model for the computation of the ionization stage against results obtained with more accurate atomic physics, and we found an overall good agreement.

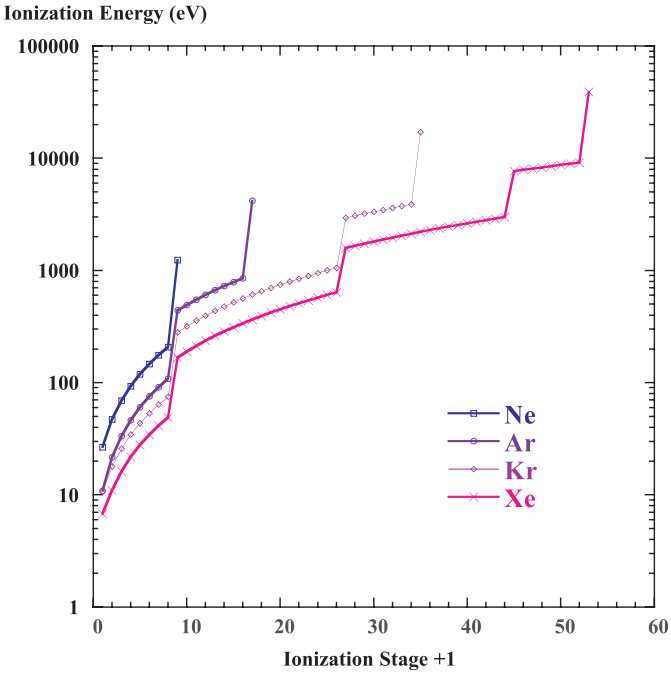

Fig. 4. Ionization energies versus the ionization stage for Ne, Ar, Kr and Xe, calculated from SHM.

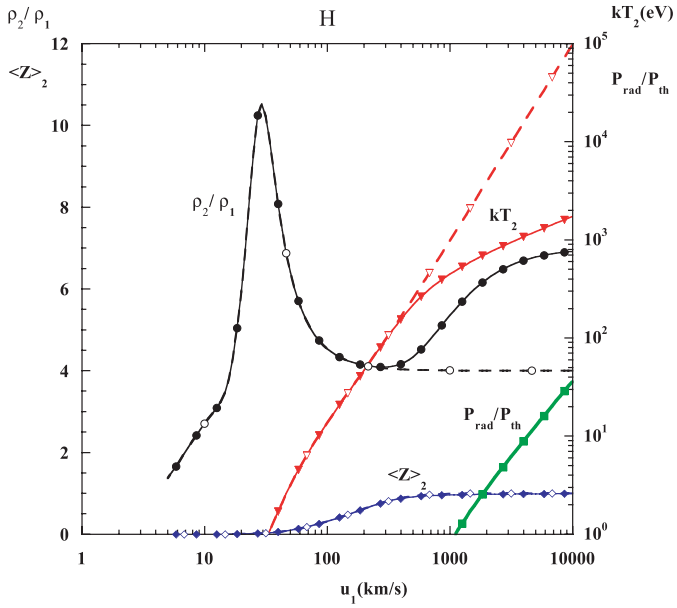

Fig. 5. Compression ρ_2/ρ_1 (thin solid line, full circles), ionization $\langle Z\rangle_2$ (diamonds), temperature T_2 (thin solid line, inverted triangles) in eV, P_{rad}/P_{th} (thick) of the shocked hydrogen gas, versus the shock velocity in $\mathrm{km\,s^{-1}}$, including radiation effects. The quantities ρ_2/ρ_1, T_2 and $\langle Z\rangle_2$ are also reported when radiation is neglected in the Rankine-Hugoniot relations (dashed lines, empty markers). Initial conditions are $kT_1 = 0.1$ eV and $\rho_1 = 5\times10^{-4}\,\mathrm{g\,cm^{-3}}$.

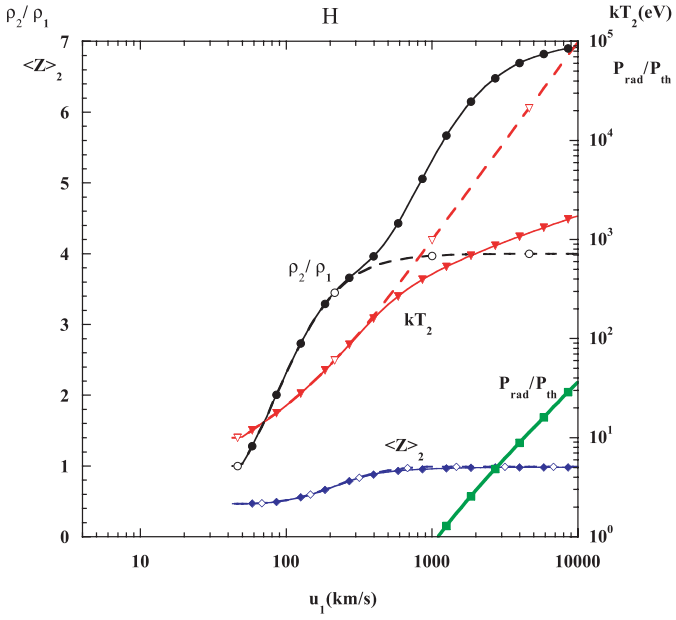

Fig. 6. Same as Figure 5 for $kT_1 = 10$ eV.

4 Shock characteristics for ionized gases

4.1 Hydrogen

In Figures 5 and 6, we analyze the influence of the radiation on the compression ratio, ρ_2/ρ_1, on the shocked temperature T_2, and on the ionization stage $\langle Z\rangle_2$ for hydrogen. We have assumed an initial density, $\rho_1 = 5\times10^{-4}\,\mathrm{g\,cm^{-3}}$, and unshocked temperatures kT_1 equal to 0.1 and 10 eV.

At $kT_1 = 0.1$ eV, the effects of atomic structure are very important, resulting in a peak of the compression ratio of 10.5 for a shock velocity of 30 $\mathrm{km\,s^{-1}}$. The compression ratio curve is very different from the case of a perfect gas (see Fig. 1). At higher temperature, we see that the strong compression peak found at $kT_1 = 0.1$ eV disappears because the initial hydrogen gas is almost fully ionized. For both initial temperatures, thermal and radiative pressures are equal for a shock velocity, $u_{rad} \approx 1100$ $\mathrm{km\,s^{-1}}$. When the radiation pressure becomes larger than the thermal pressure, the effects of the atomic structure on T_2 disappear, but they are still visible (less than 10%) in the compression ratio. Generally, the shocked temperature, T_2, is less affected by atomic physics effects than the compression ratio. At high velocities, the compression ratio tends towards a value of 7 instead of 4 when radiation is neglected. The temperature of the shocked gas is lowered when radiation is accounted for.

In Figure 7, we show that the atomic structure strongly affects the compression ratio at 0.1 eV. With a compression peak of 10.5 at shock velocity of 30 $\mathrm{km\,s^{-1}}$, this curve

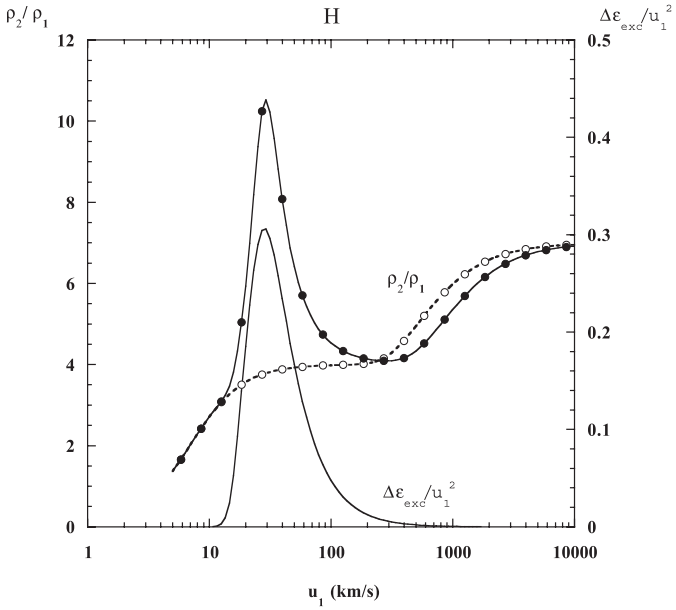

Fig. 7. ρ_2/ρ_1 (thin line, full circles), $\Delta\epsilon_{exc}/u_1^2$ (thin line, no marker) in hydrogen as ionized gas, compared to ρ_2/ρ_1 (dashed line, empty circles) in hydrogen as perfect gas. Initial conditions: $kT_1 = 0.1$ eV and $\rho_1 = 5\times10^{-4}\,\mathrm{g\,cm^{-3}}$.

differs significantly from the perfect gas curve. The compression peak is attributed to the strong increase of the excitation energy due to heating. This increase is also present when radiation is neglected. At these shock velocities, the excitation energy dominates the enthalpy term in equation (14). The radiation effects are negligible at these velocities, and the dominant terms in the left member of equation (17) are the excitation energy and the mechanical term in u_2^2. The increasing in $\Delta\epsilon_{exc} = \epsilon_{exc,2} - \epsilon_{exc,1}$ is taken from the kinetic energy (lowering thus u_2^2, see

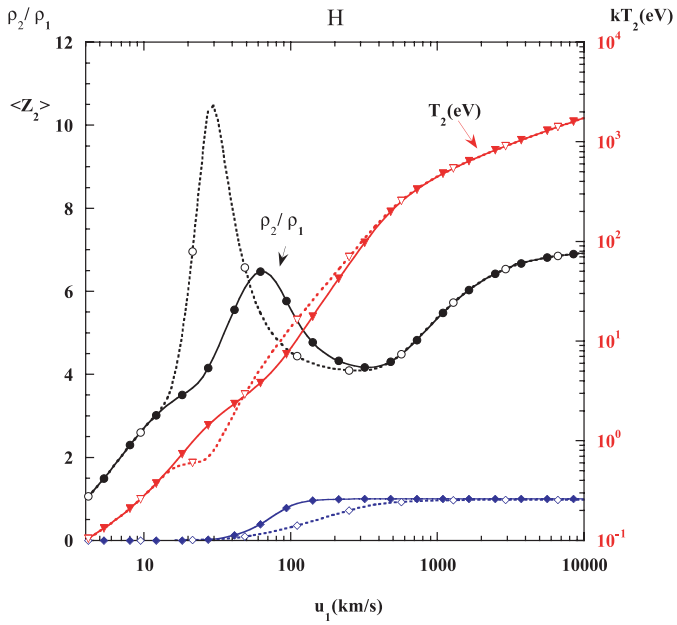

Fig. 8. ρ_2/ρ_1, $\langle Z\rangle_2$, kT_2 (eV) of the shocked gas, versus the shock velocity in $\mathrm{km\,s^{-1}}$ for hydrogen at $kT_1 = 0.1$ eV and $\rho_1 = 5\times10^{-4}\,\mathrm{g\,cm^{-3}}$. These quantities are reported for two atomic models of pure atomic hydrogen gas: detailed model (full lines, full circles for ρ_2/ρ_1 and kT_2, full diamonds for $\langle Z\rangle_2$) and SHM (dashed lines, no marker, empty diamonds for $\langle Z\rangle_2$).

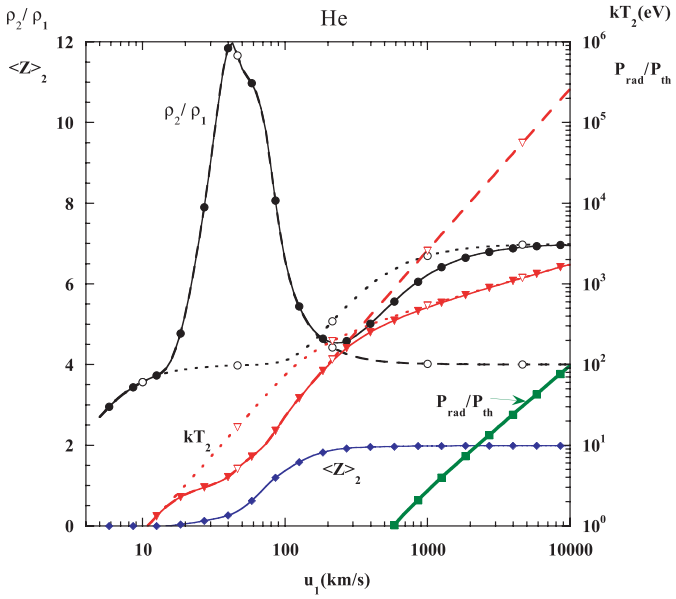

Fig. 9. ρ_2/ρ_1 (full circles, thin line), kT_2 in eV (inverted full triangles, thin line) in helium for initial conditions $kT_1 = 0.1$ eV, $\rho_1 = 5\times10^{-4}\,\mathrm{g\,cm^{-3}}$, versus shock velocity in $\mathrm{km\,s^{-1}}$, with (full markers, full lines) and without (empty markers, dashed lines) radiation. The ionization stage $\langle Z\rangle_2$ is plotted with diamonds. P_{rad}/P_{th} is plotted in thick continuous line and full squares.

Eq. (17)); due to mass conservation (Eq. (15)), this results in increasing ρ_2. The difference in excitation energy ($\Delta\epsilon_{exc}\times 96.4$, in eV), normalized to u_1^2 (u_1 in $\mathrm{km\,s^{-1}}$) is plotted together with the compression peak in Figure 7. We note that the variations of the compression ratio and excitation energy are qualitatively very similar.

In Figure 8, we illustrate the effects of the adopted atomic model on the shock description for the low initial temperature ($kT_1 = 0.1\,\mathrm{eV}$). We consider the case of a pure atomic hydrogen gas, and we use both a detailed model and the SHM. The detailed atomic model [24,25] includes the effect of pressure ionization by the formalism of level dissolution, and uses exact energies. The variations of different quantities, like ρ_2/ρ_1, T_2, $\langle Z\rangle_2$, occur in the same range of velocities. The amplitude of the compression peak differs between the two models with a value of 6.5 at $u_1 = 60\ \mathrm{km\,s^{-1}}$ for the detailed atomic model, while the compression ratio reaches a factor of 10.5 at $u_1 = 30\ \mathrm{km\,s^{-1}}$ in the SHM. As expected, the differences occur in the regime where hydrogen is partially ionized. They are due to the qualitative description of the atomic physics for hydrogen with an ionization energy of 9.7 eV instead of 13.6 eV and to a qualitative inclusion of pressure ionization effects in the SHM. The differences disappear for larger initial temperatures, because the atomic physics effects are much reduced. We have shown that the SHM yields results in good qualitative agreement with a better atomic description, and we postpone further discussion to a future paper.

4.2 Rare gases

We now turn to radiative shocks in rare gases, from helium to xenon. In this section, we choose the same initial temperatures (low, 0.1 eV, and high, 10 eV) than in hydrogen. We have also used the same initial density ($\rho_1 = 5\times10^{-4}\ \mathrm{g\,cm^{-3}}$). We have adopted the SHM since this atomic model is sufficient to describe qualitative behaviors of the shocked gas quantities, especially when considering radiative effects occurring at high temperatures, thus at large shock velocities. We have tested the pertinence of this approximation of the atomic physics against more detailed atomic models. We proceeded similarly than for hydrogen. We found that differences are negligible at high temperatures, whereas they are more important at low shock velocities and low initial temperature. In this case, the differences in compression ratio between SHM and detailed atomic models remain for helium of the same order than for hydrogen, and the differences decrease with increasing atomic number.

We have solved the GRH relations and derived shock characteristics for He, Ne, Ar, Kr and Xe. The corresponding compression ratios and temperatures are displayed in Figures 9, 11, 13, 15, 17 for the low temperature and 10, 12, 14, 16, 18 for the high initial temperature (10 eV), for the ionized gas case, with and without radiation.

The helium case is very similar to hydrogen with a peak in the compression at low temperature which vanishes at high temperature. This bump results from the excitation of neutral helium at shock velocities below 100 $\mathrm{km\,s^{-1}}$ and from the excitation of He^+ at shock

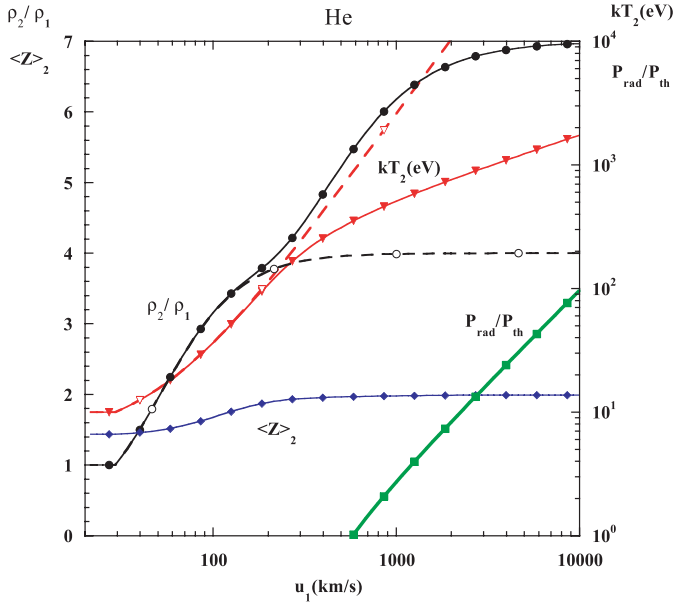

Fig. 10. Same as Figure 9 for $kT_1 = 10$ eV, $\rho_1 = 5 \times 10^{-4}$ g cm^{-3}.

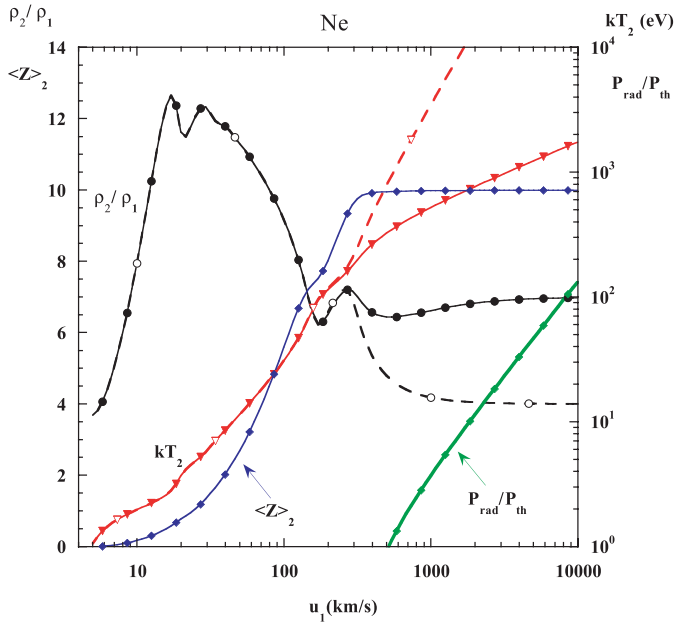

Fig. 11. Same as Figure 9 for Ne ($kT_1 = 0.1$ eV, $\rho_1 = 5 \times 10^{-4}$ g cm^{-3}).

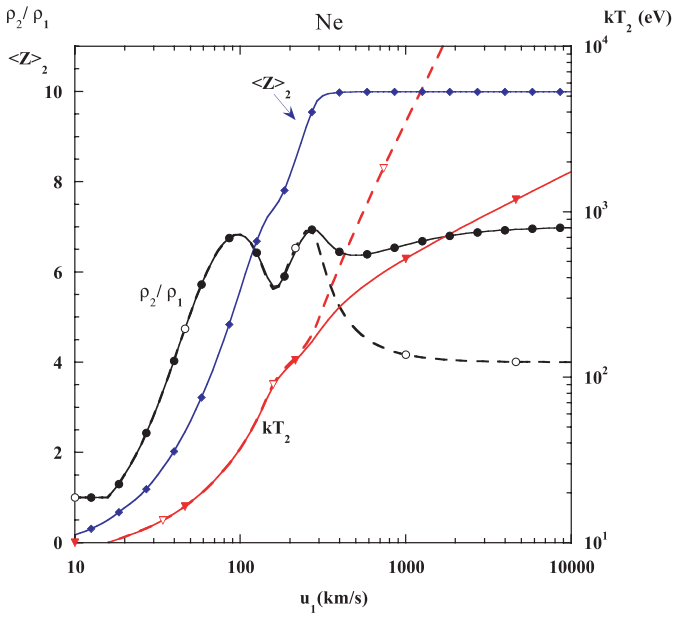

Fig. 12. Same as Figure 11 for $kT_1 = 10$ eV, $\rho_1 = 5 \times 10^{-4}$ g cm^{-3}. P_{rad}/P_{th} curve, not displayed, is very similar to the same curve in Figure 11.

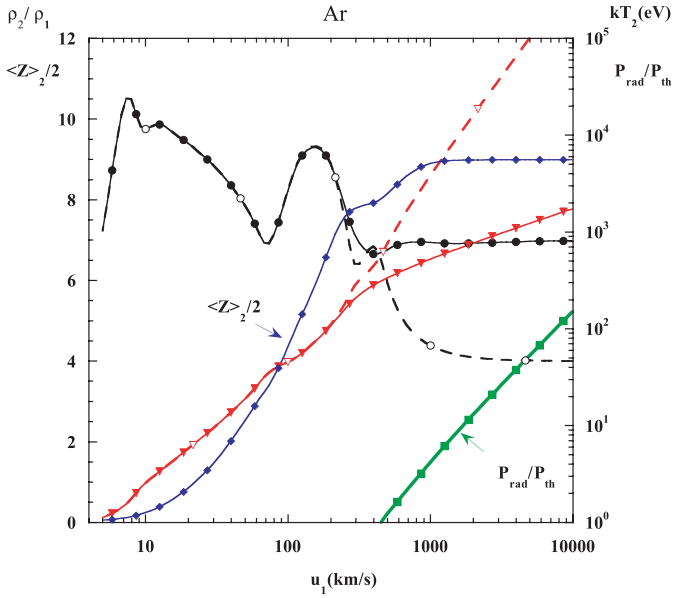

Fig. 13. Same as Figure 9 for Ar ($kT_1 = 0.1$ eV, $\rho_1 = 5 \times 10^{-4}$ g cm^{-3}).

velocities between 100 and 200 km s^{-1}. At $kT_1 = 10$ eV, the mean ionization degree is about 1.5 at low velocities, reaching the upper limit of 2 around 300 km s^{-1}. Therefore, the effect of excitation is strongly reduced for shock velocities under 200 km s^{-1}. It results that the compression ratio goes up almost monotonically towards the ratio of 7 contrary to the case at $kT_1 = 0.1$ eV where an emerging peak is visible in the compression rate, at velocities under 200 km s^{-1}.

To understand the complicate structures of the compression ratios for other rare gases, it is necessary to consider the details of the ionization energies (Fig. 4). The ionization energies show jumps related to the ionic shell structure (see an example in [26] for xenon). We might thus expect that these jumps show up in the predicted compression ratios.

As pointed out previously, the order of magnitude of the excitation energy for the shocked gas is such that it dominates the enthalpy in equation (17) and its variations are directly reflected in the term, $0.5 \times u_2^2$ of the same equation. The ratio $u_2^2/u_1^2 = \rho_1^2/\rho_2^2$ follows the variations of $\Delta\epsilon_{exc}/u_1^2$. This can been seen for example in Figure 19,

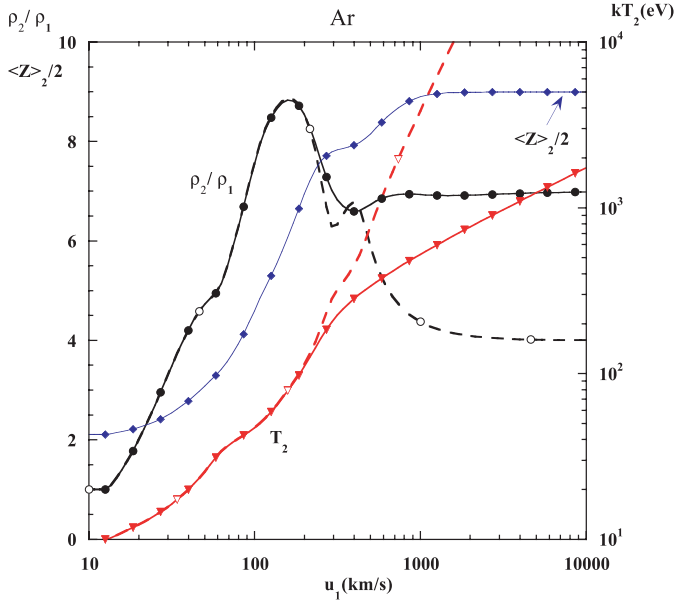

Fig. 14. Same as in Figure 13 for $T_1 = 10$ eV, $\rho_1 = 5 \times 10^{-4}$ g cm^{-3}. P_{rad}/P_{th} curve, not displayed, is very similar to the same curve in Figure 13.

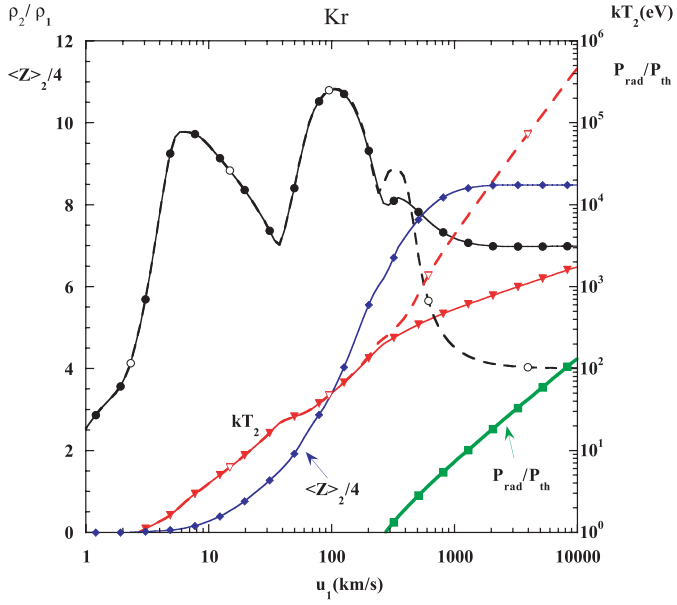

Fig. 15. Same as Figure 9 for Kr ($kT_1 = 0.1$ eV, $\rho_1 = 5 \times 10^{-4}$ g cm^{-3}).

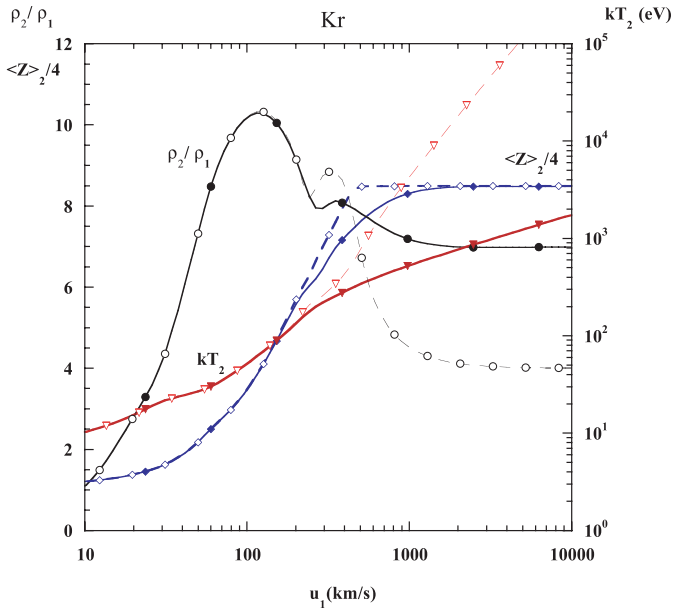

Fig. 16. Same as Figure 15 for $kT_1 = 10$ eV, $\rho_1 = 5 \times 10^{-4}$ g cm^{-3}. P_{rad}/P_{th} curve, not displayed, is very similar to the same curve in Figure 15.

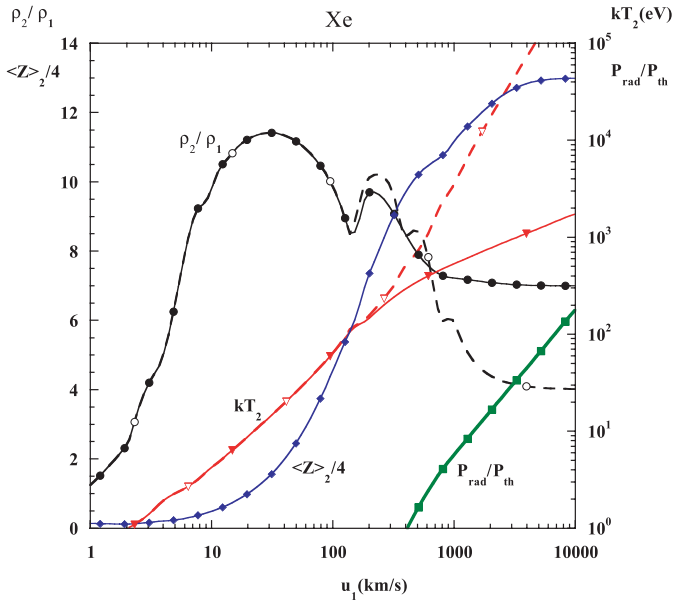

Fig. 17. Same as Figure 9 for Xe ($kT_1 = 0.1$ eV, $\rho_1 = 5 \times 10^{-4}$ g cm^{-3}).

where we have plotted the variations of the compression ratio, $\Delta\epsilon_{exc}/u_1^2$ in arbitrary units and $\langle Z\rangle_2$ for krypton at 0.1 eV. The three compression bumps at 7, 100, and 380 km s^{-1}, are visible on the normalized excitation energy variation. They follow from the variations of $\Delta\epsilon_{exc}$ and u_1^2, though the jumps in the variations of $\Delta\epsilon_{exc}$ versus u_1 are less pronounced. They are slightly visible in a change of the slope of the corresponding curve.

In the minima, the excitation energy varies less rapidly than u_1^2, and the compression ratio therefore decreases. This occurs when the gas becomes more difficult to ionize/excite and is connected to the jumps in ionization steps between atomic shells (see Fig. 4). For example, the first peak for Kr in Figure 19 ($kT_1 = 10$ eV) is associated to the progressive ionization of the outer shell, $n = 4$, and the second peak to shells, $n = 3$, and $n = 2$ (the configuration of the ground state of Kr I is ($1s^2$, $2s^2$, $2p^6$, $3s^2$, $3p^6$, $3d^{10}$, $4s^2$, $4p^6$). We can see in Figure 19 that the mean ionization degree of Kr varies between 0 and 7 for shock velocities from 1 to 35 km s^{-1}, which corresponds to an excitation/ionization of $n = 4$ shell. Let us note that it is the mean ionization degree divided by four ($\langle Z\rangle_2/4$) which

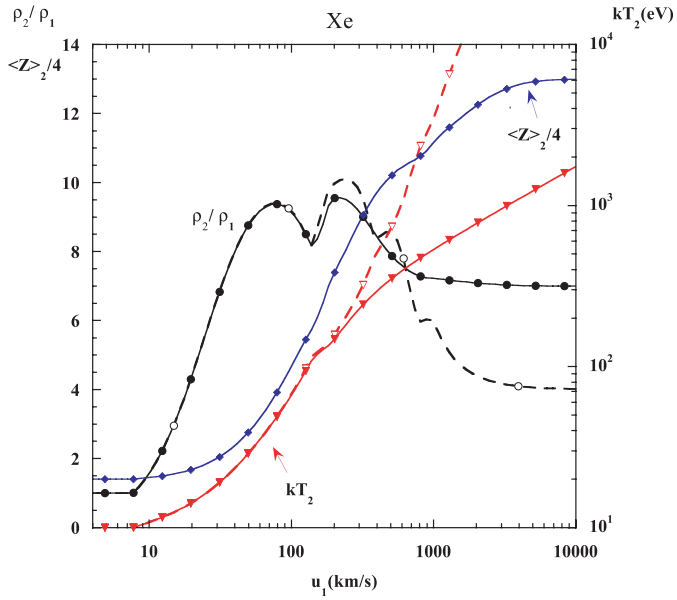

Fig. 18. Same as Figure 17 for $kT_1 = 10$ eV, $\rho_1 = 5 \times 10^{-4}$ g cm^{-3}. P_{rad}/P_{th} curve, not displayed, is very similar to the same curve in Figure 17.

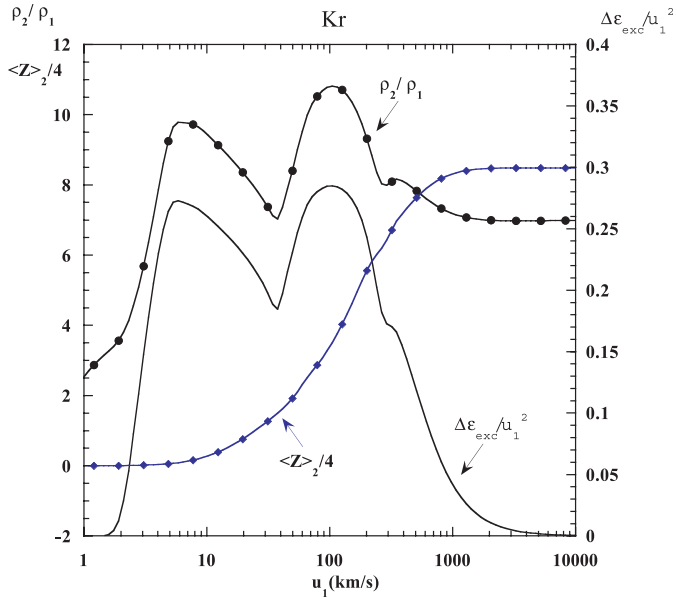

Fig. 19. ρ_2/ρ_1 (full circles), $\langle Z \rangle_2$ (full diamonds), normalized excitation energy ($\Delta\epsilon_{exc}/u_1^2$) in krypton (no marker) for initial conditions $kT_1 = 0.1$ eV, $\rho_1 = 5 \times 10^{-4}$ g cm^{-3}, versus shock velocity in km s^{-1}.

is reported in the figure in order to fit the axis scale. The second peak, between 35 and 200 km s^{-1} corresponds to the variation of the ionization stage between 8 and 25 and is associated to the $n = 3$ shell. The last small bump is related to $n = 2$ and $n = 1$ shells, and is more pronounced when radiation is accounted for.

In the energy range considered, the initial temperatures are far below the necessary energy to fully ionize the studied rare gases (i.e., 73 eV, 2121 eV, 9739 eV, 56482 eV and 154090 eV, for He, Ne, Ar, Kr and Xe, respectively), explaining therefore the strong influence of the excitation energy.

Table 1. Shock velocity u_{rad} (in km s^{-1}) for which $P_{th} = P_{rad}$. Top, perfect gas (PG); bottom, ionized gas (IG). Initial conditions are: $kT_1 = 0.1$ eV, $\rho_1 = 5 \times 10^{-4}$ g cm^{-3}.

	H	He	Ne	Ar	Kr	Xe
u_{rad} (PG)	720	286	97	63	37	28
u_{rad} (IG)	1100	580	515	450	300	410

Table 2. u_ρ and u_T at the same temperature and density for different gases ($kT_1 = 0.1$ eV, $\rho_1 = 5 \times 10^{-4}$ g cm^{-3}).

	H	He	Ne	Ar	Kr	Xe
u_ρ	450	300	300	250	250	200
u_T	400	300	250	220	220	200

4.3 Discussion

Different criteria may be defined to quantify radiation effects on macroscopic quantities in the shocked gas.

- A first possibility is the equality of thermal and radiative pressures, which defines the velocity u_{rad}. Values of this velocity are reported in Table 1 for the real and perfect gas cases of the different species. In the case of the real rare gas, we find that u_{rad} stays in the range of 500 km s^{-1} with increasing atomic number. When the criteria is lowered to $P_{rad}/P_{th} = 0.1$, the velocities are equal, in the case of the ionized gas, to 490, 260, 270, 250, 210 and 180 for H, He, Ne, Ar, Kr and Xe, respectively. They are approximatively smaller by a factor of 2.
- Alternatively, we may determine the shock velocity u_ρ for which the compression ratios ρ_2/ρ_1 differ by a given factor (say 10%), if radiation is included or not in the calculation.
- A final choice is to use the mimimum velocity, u_T, for which the shocked temperatures T_2 differ by 10% when radiation is included or not in the calculation. The corresponding velocities u_T and u_ρ are reported in Table 2 for an initial temperature of 0.1 eV and a gas density of 5×10^{-4} g cm^{-3}. These two quantities are quite similar. They are smaller than u_{rad} and decrease with increasing gas mass.

We now examine the variations of u_{rad} with the initial temperature and density.

- From equation (10) derived for the case of perfect gas, we expect that u_{rad} does not vary with T_1. However, the radiative effects in the unshocked gas should become more important as temperature increases. When the radiative pressure equals the thermal pressure in the unshocked gas, u_{rad} will tend to zero because the condition $P_{rad}/P_{th} = 1$ is already satisfied at initial conditions. The radiative pressure therefore dominates

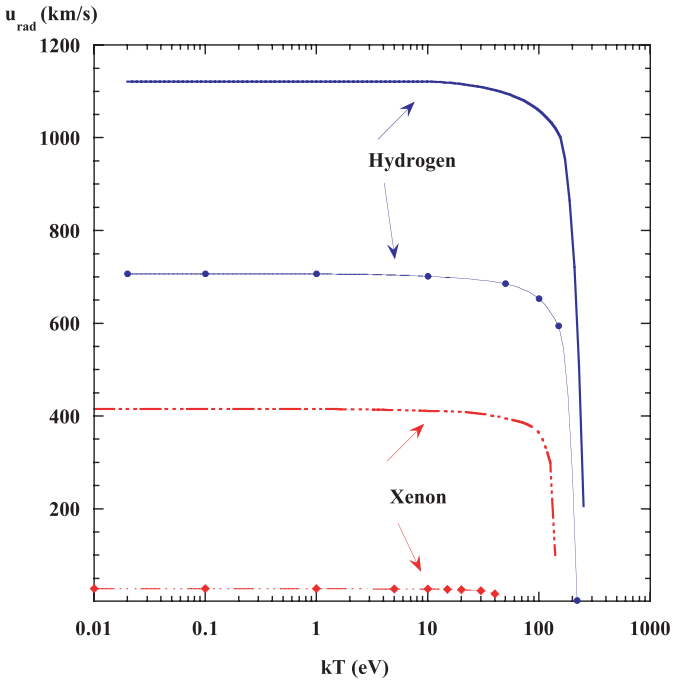

Fig. 20. Shock velocity u_{rad} in $\mathrm{km\,s^{-1}}$ for which $P_{rad} = P_{th}$ for hydrogen (full lines) as a perfect gas (full circles) and as a ionized gas (no marker) at 5×10^{-4} $\mathrm{g\,cm^{-3}}$, compared with xenon (dot-dashed lines) as a perfect gas (full diamonds) and as a ionized gas (no marker) at 5×10^{-4} $\mathrm{g\,cm^{-3}}$. Molecular equilibrium of H is taken into account in the case of the ionized gas.

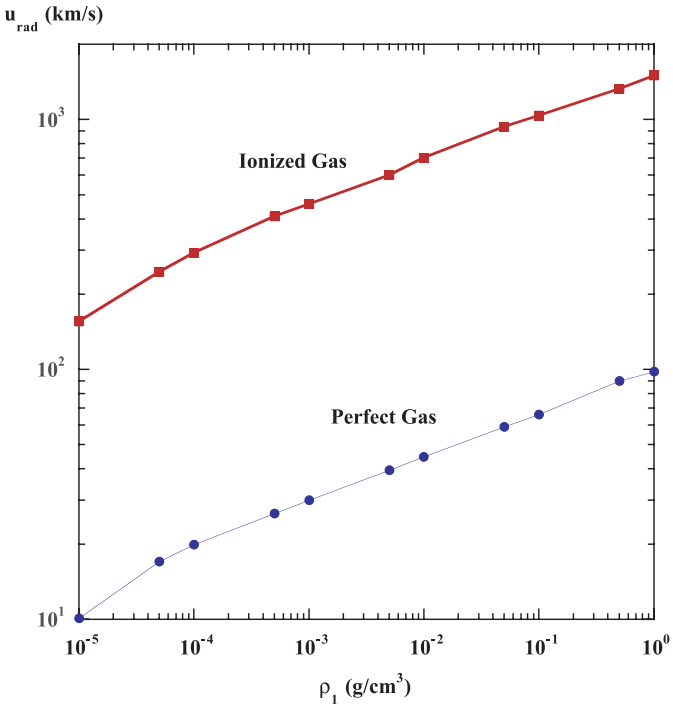

Fig. 21. Variations with ρ_1 of the shock velocity u_{rad} in $\mathrm{km\,s^{-1}}$ in xenon as a perfect gas (thin line) and as a ionized gas (thick line). Initial temperature is $kT_1 = 0.1$ eV.

the hydrodynamics before and after the shock. This limit occurs for the perfect gas at a temperature, $T_{\rm lim}$, defined by

$$T_{\rm lim} = \left(\frac{3\rho R}{aA}\right)^{1/3}, \qquad (19)$$

which corresponds to 220 eV for hydrogen and 43 eV for xenon at $\rho_1 = 5 \times 10^{-4}$ $\mathrm{g\,cm^{-3}}$. This limit is larger in the case of ionized gas. The corresponding variations for hydrogen and xenon are reported in Figure 20.

– From equation (10), we note that u_{rad} varies as $\rho^{1/6}$. In Figure 21, we have studied numerically the variations of u_{rad} with the initial density in the case of xenon at $kT_1 = 0.1$ eV. The two curves indicate a linear variation with $\rho^{1/6}$, extending the relation obtained for the perfect gas to ionized gases.

5 Conclusions

Radiation hydrodynamics calculations are generally performed assuming a perfect gas. In this paper, we have developed a simple radiative shock model where we explore extensively the differences between perfect and real gases, namely the effects of excitation, ionization, radiation energy and pressure, on the jump conditions in hypersonic shocks. We have assumed a large total optical depth, with very small photon mean path and thus negligible radiative flux, LTE, stationarity, 1-D geometry, pure gases, and no magnetic field. Our model thus provides the macroscopic conditions in the post-shock region, far from the shock, relative to the initial conditions. Compared to the perfect gas case, we found that the excitation energy becomes the dominant term in the ionized gas case, and directly affects the compression ratio. Lower initial (pre-shock) densities or higher initial temperatures result in larger radiative effects that are best evidenced in the compression ratio and in the shocked gas temperature. We have presented quantitative estimates for several rare gases which are most often used in experimental settings. For example, for xenon at an initial density of 5×10^{-4} $\mathrm{g\,cm^{-3}}$ and $kT_1 = 0.1$ eV, we found that radiation effects dominate in shocks with velocities larger than 120 $\mathrm{km\,s^{-1}}$. This limit is *significantly* higher than the value predicted from the Bouquet et al. model [14], assuming a perfect gas. This conclusion is crucial in designing future radiative shocks experiments, at energies which are large enough to transcend the excitation and ionization of the gas. At these high energies, shocks will be fully structured by radiation. Such high energies and shock velocities will be reachable with future high-power lasers (LIL, LMJ in France or NIF in the USA), which will therefore provide the necessary experimental setup to study radiative shocks.

The authors thank K. Eidman for his precious help in this study, J.P.C. Chièze, S. Bouquet, M. Cornille and D. Gilles for helpful discussions. This work was supported by the French National CNRS program of stellar physics (PNPS). T. Lanz acknowledges the support of Observatoire de Paris.

References

1. D. Mihalas, B. Weibel-Mihalas, *Foundations of Radiation Hydrodynamics* (Dover Pub. Inc., Mineola, New York, 1999)
2. A.B. Fokin, D. Gillet, Astron. Astrophys. **325**, 1013 (1997)
3. P. Mathias, D. Gillet, A. Lebre, Astron. Astrophys. **341**, 853 (1999)
4. M. Scholz, P.R. Wood, Astron. Astrophys. **362**, 1065 (2000)
5. C. Stehlé, J.P. Chièze, *Scientific Highlights 2002*, edited by D. Barret, F. Combes (EDP-Sciences, Les Ulis, 2002), p. 493
6. H.A. Bethe, Astrophys. J. **490**, 765 (1997)
7. A. Calder, B. Fryxell, T. Plewa, R. Rosner, L.J. Dursi, V.G. Weirs, T. Dupont, H.F. Robey, J.O. Kane, B.A. Remington, R.P. Drake, G. Dimonte, M. Zingale, F.X. Timmes, K. Olson, P. Ricker, P. MacNeice, H.M. Tufo, Astrophys. J. Suppl. **143**, 201 (2002)
8. K. Shigemori, R. Kodama, D.R. Farley, T. Koase, K.G. Estabrook, B.A. Remington, D.D. Ryutov, Y. Ochi, H. Azechi, J. Stone, N. Turner, Phys. Rev. E **62**, 8838 (2000)
9. J.M. Laming, J. Grun, Phys. Rev. Lett. **89**, 125002 (2002)
10. K.S. Budil, M. Gold, K.G. Estabrook, B.A. Remington, J. Kane, P.M. Bell, D.M. Pennington, C. Brown, S.P. Hatchett, J.A. Koch, M.H. Key, M.D. Perry, Astrophys. J. Suppl. **127**, 261 (2000)
11. X. Fleury, S. Bouquet, C. Stehlé, M. Koenig, D. Batani, A. Benuzzi-Mounaix, J.-P. Chièze, N. Grandjouan, J. Grenier, T. Hall, E. Henry, J.-P.J. Lafon, S. Leygnac, B. Marchet, H. Merdji, C. Michaut, F. Thais, Las. Part. Beams **20**, 263 (2002)
12. P.A. Keiter, R.P. Drake, T.S. Perry, H.F. Robey, B.A. Remington, C.A. Iglesias, R.J. Wallace, J. Knauer, Phys. Rev. Lett. **89**, 165003 (2002)
13. J.E. Bailey, G.A. Chandler, S.A. Slutz, G.R. Bennett, G. Cooper, J.S. Lash, S. Lazier, R. Lemke, T.J. Nash, D.S. Nielsen, T.C. Moore, C.L. Ruiz, D.G. Scroen, R. Smelser, J. Torres, R.A. Vesey, Phys. Rev. Lett. **89**, 095004 (2002)
14. S. Bouquet, R. Teyssier, J.-P. Chièze, Astrophys. J. Suppl. **127**, 245 (2000)
15. Ya.B. Zel'dovich, Yu.P. Raizer, *Physics of Shock Waves and high-Temperature Hydrodynamic Phenomena*, edited by W.D. Hayes, R.F. Probstein (Dover Pub. Inc., Mineola, New York, 2001)
16. S.I. Pai, A.I. Speth, Phys. Fluid. **4**, 1232 (1961)
17. R.A. Alpher, H.D. Greyber, Phys. Fluid. **1**, 160 (1958)
18. R.G. Sachs, Phys. Rev. **69**, 514 (1946)
19. H. Nieuwenhuijzen, C. de Jager, M. Cuntz, A. Lobel, L. Achmad, Astron. Astrophys. **280**, 195 (1993)
20. K. Eidmann, Las. Part. Beams **12**, 223 (1994)
21. B. Kärcher, *Atomphysikalische Beschreibung Ionenstrahl-erzeugter Plasmen* (MPQ report, 1991), p. 158
22. R.M. More, Adv. At. Mol. Phys. **21**, 305 (1985)
23. G.C. Pomraning, *The equations of Radiation Hydrodynamics* (Pergamon Press, Oxford, 1973)
24. C. Stehlé, S. Jacquemot, Astron. Astrophys. **271**, 348 (1993)
25. D.G. Hummer, D. Mihalas, Astrophys. J. **331**, 794 (1988)
26. C. Michaut, L. Boireau, M. Cornille, S. Leygnac, C. Stehlé, *Scientific Highlights 2002*, edited by D. Barret, F. Combes (EDP-Sciences, Les Ulis, 2002), p. 543